Multiple localized states in centrifugally stable rotating flow

J. Abshagen,[1,a)] M. Heise,[1] G. Pfister,[1] and T. Mullin[2]
[1]Institute of Experimental and Applied Physics, University of Kiel, 24098 Kiel, Germany
[2]School of Physics and Astronomy, The University of Manchester, Manchester M13 9PL, United Kingdom

(Received 6 December 2009; accepted 21 January 2010; published online 26 February 2010)

We report experimental and numerical results from investigations into the onset of novel localized cellular states in the centrifugally stable regime of Taylor–Couette flow at sufficiently high rates of counter-rotation of the outer cylinder. Quantitative comparison is made between experimental results and those obtained from numerical bifurcation studies of the steady axisymmetric Navier–Stokes equations. The onset of the vortices is smooth but they appear over a narrow range of Reynolds number. This enables the use of a suitable measure to produce excellent quantitative agreement between calculation and experiment. The numerical methods are also used to uncover evidence for a homoclinic snake which indicates rich multiplicity in the steady solution set. © *2010 American Institute of Physics*. [doi:10.1063/1.3326076]

Multiplicity of states is an interesting aspect of nonlinear physical systems which has been the focus of research in a number of areas of fluid dynamics including plasmas,[1] atmospheric dynamics,[2] rotating flows,[3,4] convection,[5–7] and flow in porous media[8] and in elastic tubes.[9,10] The majority of these investigations have been carried out in parameter regimes where the base state is unstable and pattern formation instabilities[11] are prevalent. In these situations the multiple fixed points are believed to form the backbone of more complicated motions found in neighboring parameter ranges.

More recently, multiplicity has been uncovered in the form of localized states of spatially extended systems in problems arising in nonlinear optics,[12] magnetic fluids,[13] binary mixture convection,[14] and models of cardiovascular calcification.[15] These states arise on a so-called "homoclinic snaking" branch[16,17] which bifurcates subcritically from a trivial state. Each fold in the snake corresponds to different spatially localized state so that, in principle, a large number of states can coexist.

Here we report the experimental and numerical results on the spontaneous appearance of novel steady vortex states which appear below the well-known centrifugal instability of counter-rotating Taylor–Couette flow toward time-dependent, nonaxisymmetric spiral vortices.[18] The novel type of vortices presented here is steady and axisymmetric and has a much smaller length scale than classical Taylor cells. Excellent agreement is found between the results of the experimental observations and the numerical calculations and we also use the numerical techniques to provide evidence for homoclinic snaking.

The experimental measurements were performed in a Taylor–Couette apparatus with a rotating inner (radius r_i) and counter-rotating outer (r_o) cylinder and nonrotating end walls at the top and bottom. Hence the flow took place in the annular gap between the two cylinders which had an axial length L. The control parameters were the Reynolds number of the inner and outer cylinders $\mathrm{Re}_{i,o}=\Omega_{i,o}dr_{i,o}/\nu$, with $\Omega_{i,o}$ denoting the rotation rate of the inner and outer cylinders, respectively, ν the kinematic viscosity, and $d=r_o-r_i$ the gap width (length is scaled with d). Geometric parameters were the aspect ratio $\Gamma=L/d$ and the radius ratio $\eta=r_i/r_o=0.5$. Specifications of the experimental setup were $r_i=(12.50\pm0.01)$ mm, $r_o=(25.00\pm0.01)$ mm, $\nu=(11.9\pm0.1)$ cS, and $\Delta L=0.01$ mm. Feedback control of the motors enabled an accuracy in Re of $\Delta\,\mathrm{Re}/\mathrm{Re}\propto10^{-4}$ during a measurement.

We utilize laser-Doppler velocimetry (LDV) for measurements of either the axial (v_z) or the radial component (v_r) of the velocity at selected positions in the flow domain. The positioning accuracy of the LDV system in the flow is 10 μm in each direction but the spatial resolution is limited by the size of the measurement volume, i.e., about 300 and 800 μm in axial/radial and in azimuthal direction, respectively. Our LDV allows measurements of velocities from 10 μm s^{-1} to 10 cm s^{-1}. The accuracy can be improved by averaging in steady flows.

In the numerical calculations, the steady Navier–Stokes equations with no-slip boundary conditions were solved for axisymmetric flows using the software suite ENTWIFE.[19] Standard procedures enabled the continuation of solution branches and calculations of bifurcation points enabled paths of saddle nodes to be followed as a function of the control parameters together. The computational domain was a full cross section of the annular gap between the two cylinders with stationary end walls. The full domain was discretized using a 240×10 and 200×20 finite-element mesh which was uniform over most of the domain. Suitable corner refinements were employed to take into account the rapid change in velocity between the moving and stationary walls in the corners. The finite elements were nine-node quadrilaterals with biquadratic velocity and discontinuous linear pressure interpolation. As a check on accuracy, the number of elements in each direction was doubled, and this produced less than a 0.01% change in the calculation of a saddle-node bifurcation point.

In many studies of Taylor–Couette flow, the outer

[a)]Electronic mail: abshagen@physik.uni-kiel.de.

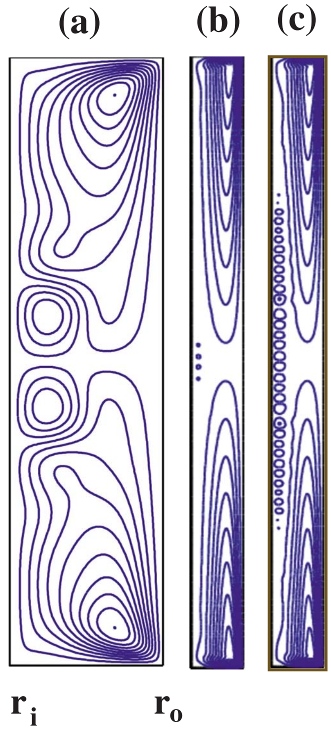

FIG. 1. (Color online) Streamline plots of cellular states calculated at (a) $\Gamma=4$ and $\mathrm{Re}_{i,o}=(150,-300)$ and [(b) and (c)] $\Gamma=12$, $\mathrm{Re}_{i,o}=(365,-1825)$, and $\mathrm{Re}_{i,o}=(408,-2040)$.

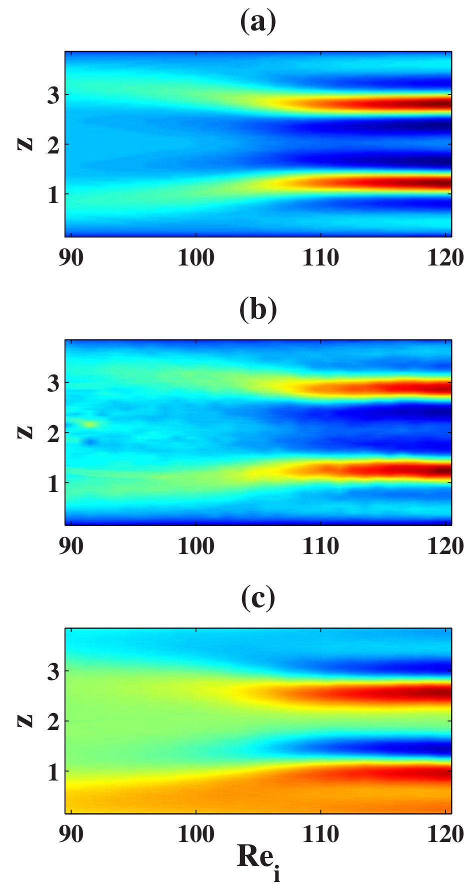

FIG. 2. (Color online) The onset of cellular states at $\Gamma=4$ and $\mathrm{Re}_o=-116.6$: [(a) and (b)] calculated and measured radial velocity profiles $v_r(\vec{r}\in I)$ within the interval $I=(r=r_i+0.08,\ \phi=\text{const},\ z\in[0.15:3.85])$, respectively, and (c) measured axial velocity profiles $v_z(\vec{r}\in I)$.

boundary is stationary and the Ekman cells formed adjacent to each end boundary are comparable in size to Taylor cells. A distinctive feature of the flow fields shown in Fig. 1 is the symmetric large-scale two cell circulations such that the flow is directed inward at each end and outward at the axial midplane.[20] These large-scale flows can be seen for both $\Gamma=4$ and $\Gamma=12$ and were found over a wide range of $\mathrm{Re}_{i,o}$. The new localized cellular states appeared in addition to the background circulation above a well-defined range of $\mathrm{Re}_{i,o}$. Examples of these cellular states are shown in Fig. 1 which were calculated for parameter values of (a) $\Gamma=4$, $\mathrm{Re}_{i,o}=(150,-300)$, (b) $\Gamma=12$, $\mathrm{Re}_{i,o}=(365,-1825)$, and (c) $\Gamma=12$, $\mathrm{Re}_{i,o}=(408,-2040)$. The small vortices always appeared close to the inner cylinder and they are both axisymmetric and symmetric about the midplane.

The onset of the new state was initiated by the appearance of weak streamwise vortices close to the axial midplane, as in the example shown in Fig. 1(b) for $\Gamma=12$. It can also be seen that a 20% increase in $\mathrm{Re}_{i,o}$ resulted in the formation of a column of almost equally sized streamwise vortices. They extend across approximately 25% of the gap at $\mathrm{Re}_{i,o}=(408,-2040)$ and spread preferentially along rather across the gap with increasing Re_i. Hence, the vortices shown in Fig. 1(c) spread along the cylinder but remain close to it. In practice, this makes the flow visualization of the streamwise vortices difficult.

The development of the localized cellular state with Re_i is illustrated in Fig. 2. Here, axial profiles of the radial [(a) and (b)] and axial (c) velocity are shown for fixed $\mathrm{Re}_o=-116.6$ and a range of Re_i at $\Gamma=4$. Since the vortices appeared close to the inner cylinder, profiles measured within the interval $I=(r=r_i+0.08,\ \phi=\text{const},\ z\in[0.15:3.85])$ provided a good estimate of the flow state.

Two pronounced outward jets can be seen to emerge symmetrically about the midplane when Re_i is increased, shown in Figs. 2(a) and 2(b). This can also be seen in axial velocity profiles depicted in Fig. 2(c). The numerical investigations reveal that the cellular states emerge with increasing Re_i without passing through a bifurcation point, but the observed qualitative change in the flow pattern occurs over a well-defined small range of Re_i.

A quantitative measure which was found to provide a good estimate of the onset of cellular motion is related to the spatial mean of a squared velocity component, i.e., $k_n \equiv \langle v_n^2(\vec{r}\in I)\rangle$ with $n=r,z$. Below the onset k_n is found to increase linearly which results from a strengthening of the large-scale circulation with increasing Re_i. The onset of cellular states is determined from the departure from this linear growth, i.e., by $\delta k_n \equiv (k_n-\tilde{k}_n)/K_n$. Here, $\tilde{k}_n \equiv \alpha\,\mathrm{Re}_i + k_0$ is obtained from a linear fit to k_n within an interval of Re_i below the onset, e.g., within $\mathrm{Re}_i\in[90:99]$ for the measurement presented in Fig. 3, and $K_n \equiv [\Sigma_{\mathrm{Re}_i=90}^{120}(k_n-\tilde{k}_n)\Delta\,\mathrm{Re}_i]$ is a normalization constant which was necessary to enable comparison between numerics and experiments. Note that in the experiment $K_r=K_z$ to within the measurement errors.

In Fig. 3 the normalized difference δk_n obtained from

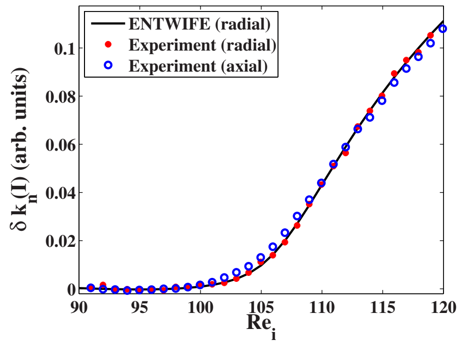

FIG. 3. (Color online) The onset of cellular states at $\mathrm{Re}_o=-116.6$ and $\Gamma=4$: departure δk_n in mean-square velocity from linear growth of large scale circulation with Re_i. The velocity components were measured and calculated at a location on the centerline and 0.08 from the inner cylinder. All curves are normalized but with the same constant for radial and axial velocity components in the experiment.

both measurements and numerical calculations at $\Gamma=4$ and $\mathrm{Re}_o=-116.6$ is shown plotted versus Re_i. The velocity components were measured and calculated at a location on the centerline and 0.08 from the inner cylinder wall. It can be seen that good quantitative agreement between numerics and experiments is found. The onset of cellular states occurs at relatively well-defined values of Re_i, as may be seen in Fig. 3. An estimate of a "critical" value was determined quantitatively by a curve fitting procedure.

A comparison between numerical and experimental results for the onset of cellular states at $\Gamma=4$ is shown in Fig. 4 over a range of $\mathrm{Re}_{i,o}$. Good quantitative agreement is found and it can also be seen that the onset of the new vortex states always lies significantly below the well-known linear instability of circular Couette flow for both Taylor cells and spiral vortices (with $m=1$). In particular it may be seen in Fig. 4 that the departure from the linear stability curve increases with decreasing Re_o. The linear stability curve was calculated with the usual assumption of cylinders of infinite length, i.e., for circular Couette flow.

The numerical continuation methods are now used to explore a complex bifurcation sequence which the new cellular states can undergo. It should be noted that these bifurcation sequences are found at control parameter values which are below the linear instability curve of circular Couette flow. An example of such a homoclinic snaking bifurcation sequence calculated along a path with a set speed ratio of $\Omega_o/\Omega_i=-2$ is given for $\Gamma=4.0$ in Fig. 5. Centrifugal instability with $m=0$ for circular Couette flow with $\eta=0.5$ occurs at $\mathrm{Re}_i=434$ for this speed ratio.

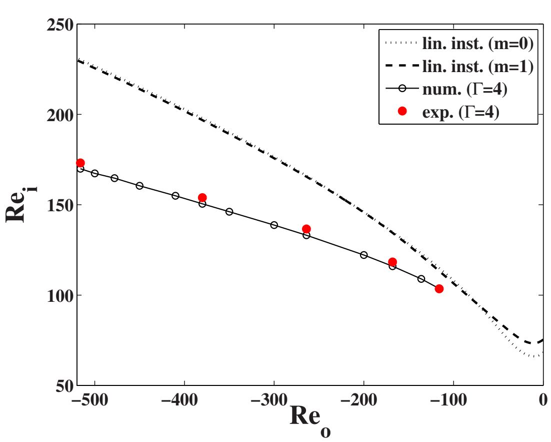

FIG. 4. (Color online) Comparison between numerical and experimental results for the onset of the new cellular states in counter-rotating Taylor–Couette flow at $\Gamma=4$.

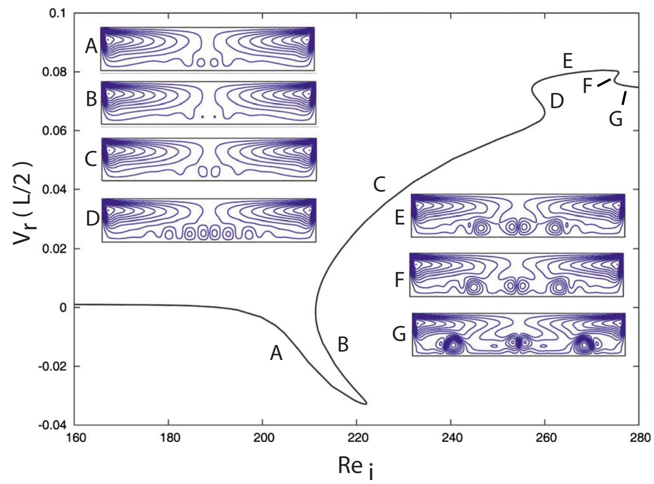

FIG. 5. (Color online) Bifurcation diagram of localized states along the path of speed ratio $\Omega_i/\Omega_o=-2$. Folds between states A and B as well as B and C occur close to the onset as a part of a cusp bifurcation. Strongly localized states E, F, and G appear in a snake in phase space above the onset of cellular states but well below the centrifugal instability. The measure used to distinguish the flow is the radial velocity component located at the midplane and 0.08 from the inner cylinder.

Increasing Re_i above the onset along this path, state A appears smoothly from the flow with two large-scale vortices at $\mathrm{Re}_i=214.2$. As Re_i is increased to $\mathrm{Re}_i=222.131\,92$ a fold is encountered and the state labeled B emerges. The process repeats through a fold at $\mathrm{Re}_i=211.303\,49$ where state C is found and subsequently states D, E, F, and G arise at $\mathrm{Re}_i=259.993\,07$, $257.269\,99$, $275.712\,57$, and $274.789\,87$, respectively. The initial fold between states A and B is a path through a cusp which originates at $\mathrm{Re}_i=208.917\,53$ and $\Gamma=4.966\,504\,8$ at this speed ratio. The wiggle is distorted by the combination of the path chosen to pass through parameter space and the measure used to distinguish the states (here the radial velocity measured at the axial middle at the radial position of 0.08 from the inner cylinder). The snake produces a sequence of localized states A, B, C, D, E, and F where each is separated by a saddle node bifurcation. This provides a mechanism for the appearance of multiple localized states.

The novel flow states we have uncovered consist of axisymmetric vortices which emerge close to the inner cylinder when Re_i is increased above a relatively well-defined but noncritical value. Close to the onset, the streamwise vortices are located in the vicinity of the axial midplane, but at higher Re_i they spread in the axial direction so that a vortex column is formed over the length of the cylinder. The new states appear in the presence of large-scale weak circulations which are a feature of finite-length effects in counter-rotating Taylor–Couette flow. They are not found if the calculations are performed on an axially periodic domain where the base state is rotary Couette flow. Hence the background circulation is an important and salient feature of the flow. This aspect makes them distinct from other examples of homoclinic snaking which have been reported to date.[16,17,21] Moreover, the new states appear significantly below the centrifugal instability of counter-rotating Taylor–Couette flow.

The multiple localized states presented here provide a novel class of solutions to counter-rotating Taylor–Couette flow which are likely to be present in addition to the nonaxisymmetric spiral vortices in any experiment. The latter states are recognized as the predominant primary flow state within the counter-rotating regime.[18] Multiplicity of these localized states is found in the form of homoclinic snaking, indicating that a rich solution structure exists in the experiment where stability is indicated from models based on periodic domains.

We thank J. Dawes and E. Knobloch for simulating discussions regarding homoclinic snaking and K. A. Cliffe for advice on the numerical bifurcation work. We also thank Ch. Hoffmann from Saarland University for the numerical data of the linear stability curves shown in Fig. 4 and W. Schumann for technical support. J.A., M.H., and G.P. acknowledge the financial support from Deutsche Forschungsgemeinschaft.

[1] M. Ottaviani, F. Porcelli, and D. Grasso, "Multiple states of nonlinear drift-tearing islands," Phys. Rev. Lett. **93**, 075001 (2004).
[2] I. B. Konovalov, A. M. Feigin, and A. Mukhina, "Toward understanding of the nonlinear nature of atmospheric photochemistry: Multiple equilibrium states in the high-latitude lower stratospheric photochemical system," J. Geophys. Res. **104**, 3669, doi:10.1029/1998JD100037 (1999).
[3] D. Coles, "Transition in circular Couette flow," J. Fluid Mech. **21**, 385 (1965).
[4] T. B. Benjamin and T. Mullin, "Notes on the multiplicity of flows in the Taylor experiment," J. Fluid Mech. **121**, 219 (1982).
[5] J. S. Yoo, "Transition and multiplicity of flows in natural convection in a narrow horizontal cylindrical annulus: Pr=0.4," Int. J. Heat Mass Transfer **42**, 709 (1999).
[6] B. Hof, P. G. Lucas, and T. Mullin, "Flow state multiplicity in convection," Phys. Fluids **11**, 2815 (1999).
[7] K. Boronska and L. S. Tuckerman, "Standing and travelling waves in cylindrical Rayleigh–Bénard convection," J. Fluid Mech. **559**, 279 (2006); "Extreme multiplicity in cylindrical Rayleigh–Bénard convection: I. Time-dependence and oscillations," Phys. Rev. E (in press); "Extreme multiplicity in cylindrical Rayleigh–Bénard convection: II. Bifurcation diagram and symmetry classification," *ibid.* (in press).
[8] B. Li, L. Zheng, X. Zhang, and L. Ma, "The multiple solutions of laminar flow in a uniformly porous channel with suction/injection," Adv. Studies Theor. Phys. **2**, 473 (2008).
[9] X. Y. Luo and T. J. Pedley, "Multiple solutions and flow limitation in collapsible channel flows," J. Fluid Mech. **420**, 301 (2000).
[10] A. Heap and A. Juel, "Anomalous bubble propagation in elastic tubes," Phys. Fluids **20**, 081702 (2008).
[11] M. C. Cross and P. C. Hohenberg, "Pattern formation outside of equilibrium," Rev. Mod. Phys. **65**, 851 (1993).
[12] S. Barbay, X. Hachair, T. Elsass, I. Sagnes, and R. Kuszelewicz, "Homoclinic snaking in a semiconductor-based optical system," Phys. Rev. Lett. **101**, 253902 (2008).
[13] R. Richter and I. V. Barashenkov, "Two-dimensional solitons on the surface of magnetic fluids," Phys. Rev. Lett. **94**, 184503 (2005).
[14] D. Jung and M. Lücke, "Localized waves without the existence of extended waves: Oscillatory convection of binary mixtures with strong Soret effect," Phys. Rev. Lett. **89**, 054502 (2002).
[15] A. Yochelis, Y. Tintut, L. L. Demer, and A. Garfinkel, "The formation of labyrinths, spots and stripe patterns in a biochemical approach to cardiovascular calcification," New J. Phys. **10**, 055002 (2008).
[16] E. Knobloch, "Spatially localized structures in dissipative systems: Open problems," Nonlinearity **21**, T45 (2008).
[17] J. H. P. Dawes, "Modulated and localized states in a finite domain," SIAM J. Appl. Dyn. Syst. **8**, 909 (2009).
[18] E. R. Krueger, A. Gross, and R. C. Di Prima, "On relative importance of Taylor-vortex and non-axisymmetric modes in flow between rotating cylinders," J. Fluid Mech. **24**, 521 (1966); H. A. Snyder, "The stability of rotating Couette flow. I. Asymmetric waveforms," Phys. Fluids **11**, 728 (1968); C. D. Andereck, S. S. Liu, and H. L. Swinney, "Flow regimes in a circular Couette system with independently rotating cylinders," J. Fluid Mech. **164**, 155 (1986); W. F. Langford, R. Tagg, E. J. Kostelich, H. L. Swinney, and M. Golubitsky, "Primary instabilities and bicriticality in flow between counter-rotating cylinders," Phys. Fluids **31**, 776 (1988); C. Hoffmann, M. Lücke, and A. Pinter, "Spiral vortices traveling between two rotating defects in the Taylor–Couette system," Phys. Rev. E **72**, 056311 (2005); M. Heise, J. Abshagen, K. Hochstrate, D. Küter, G. Pfister, and Ch. Hoffmann, "Localized spirals in Taylor–Couette flow," *ibid.* **77**, 026202 (2008); M. Heise, K. Hochstrate, J. Abshagen, and G. Pfister, "Spiral vortices in Taylor–Couette flow with rotating endwalls," *ibid.* **80**, 045301 (2009).
[19] K. A. Cliffe and S. J. Tavener, "Implementation of extended systems using symbolic algebra," in *Continuation Methods in Fluid Dynamics*, edited by D. Henry and A. Bergeon, Notes on Numerical Fluid Mechanics, Vol. 74 (Vieweg, Braunschweig, Germany, 2000), pp. 81–92.
[20] R. Hollerbach and A. Fournier, "End-effects in rapidly rotating cylindrical Taylor–Couette flow," AIP Conf. Proc. **733**, 114 (2004).
[21] I. Mercader, O. Batiste, A. Alonso, and E. Knobloch, "Localized pinning states in closed containers: Homoclinic snaking without bistability," Phys. Rev. E **80**, 025201 (2009).